IEEE Access
Multidisciplinary | Rapid Review | Open Access Journal

Received 20 April 2025, accepted 9 May 2025, date of publication 14 May 2025, date of current version 4 June 2025.

Digital Object Identifier 10.1109/ACCESS.2025.3569879

TOPICAL REVIEW

Recent Developments in Thermal Management of 3D ICs: A Review

FEN GUO, ZHAO-JUN SUO, XIN XI, YU BI, TUO LI, CHANGHONG WANG, KANG SU, XIAOFENG ZOU, AND RENGANG LI

Shandong Yunhai Guochuang Cloud Computing Equipment Industry Innovation Company Ltd., Jinan 250000, China
Shandong Inspur Artificial Intelligence Research Institute Company Ltd., Jinan 250013, China

Corresponding author: Rengang Li (lirg@inspur.com)

This work was supported in part by the National Key Research and Development Program of China under Grant 2023YFB4402900; and in part by the Natural Science Foundation of Shandong Province under Grant ZR2023QF040, Grant ZR2023LZH004, and Grant ZR2023LZH001.

ABSTRACT Three-dimensional integration circuits (3D ICs) have become an important direction of integrated circuits, which brings in a higher integration level, higher power density, and shorter wire length. However, the heat management challenge becomes one of the key limitations for the development of 3D integration which needs desperate solutions. To address this challenge, the researchers conducted an in-depth investigation into heat transfer technologies within key structures of 3D ICs. This paper aims to review the literature on thermal management technologies, with a particular emphasis on advancements in three critical areas: thermal interface materials (TIM), through-silicon vias (TSV), and heat sink designs. Continuous research and innovation in TIM, TSV, and heat sink structures have provided diverse approaches and technical solutions for addressing thermal management issues in 3D ICs. It is expected that this review article can help researchers in academia and industry to understand the state-of-the-art of heat transfer in 3D ICs and provide better research ideas.

INDEX TERMS Three-dimensional integrated circuits, thermal management, TSV, heat sinks.

I. INTRODUCTION

The relentless miniaturization of integrated circuits has propelled the semiconductor industry into the era of three-dimensional (3D) integration, where vertical stacking of multiple device layers enables unprecedented performance and energy efficiency [1]. A 3D integrated circuit (3D IC), characterized by its multilayer architecture interconnected through through-silicon vias (TSVs), achieves significant enhancements in integration density and signal transmission speed. However, this architectural advancement intensifies thermal management challenges due to vertically concentrated power densities, material thermal resistance limitations, and spatially constrained heat dissipation pathways. Central to these challenges are three critical structural components: thermal interface materials (TIMs), TSVs, and heat sinks. Their thermal performance fundamentally dictates the reliability and scalability of 3D systems, yet each component faces intrinsic limitations governed by material physics and structural design trade-offs. Figure 1 illustrates the typical structure of a 3D lC, which includes key components such as the substrate, C4 bumps, chip device layers, TlM, micro bumps, heat spreader, and heat sink.

TIMs serve as interfacial layers to mitigate contact thermal resistance by filling microscopic gaps between heterogeneous material interfaces. Despite their critical role in heat transfer between stacked dies and heat sinks, conventional polymer-based TIMs exhibit limited thermal conductivity (<5 W/(m·K)) and interfacial thermal resistances as high as 5–10 K·mm^2/W due to bond-line thickness variations and void formation during bonding processes [2]. Advanced composites incorporating silver nanoparticles (AgNPs) or graphene fillers face unresolved trade-offs: AgNP-TIMs introduce parasitic capacitance that degrades high-frequency signal integrity, while graphene-enhanced TIMs suffer from anisotropic thermal conductivity (>20 W/(m·K) in-plane vs.

The associate editor coordinating the review of this manuscript and approving it for publication was Wen-Sheng Zhao.

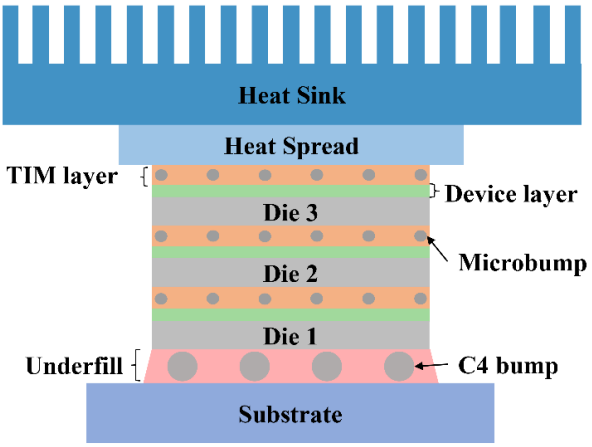

FIGURE 1. Schematic of the typical 3D IC.

<5 W/(m·K) through-plane) due to alignment challenges [3], [4]. Additionally, coefficient of thermal expansion (CTE) mismatches between TIMs and silicon substrates generate cyclic shear stresses [2], [5].

TSVs are categorized into power, signal, and thermal TSVs (TTSVs) to address distinct functional requirements [6] [7]. While power and signal TSVs facilitate interlayer electrical connectivity, TTSVs are specifically designed to mitigate thermal bottlenecks by transferring heat to heat sinks. Copper-filled TSVs achieve axial thermal conductivities up to 400 W/(m·K); however, their radial thermal conductivity plummets to <10 W/(m·K) due to interfacial voids and diffusion barrier layers. This anisotropy induces lateral temperature gradients of 20–30°C across 5 mm^2 die areas. Furthermore, spatial competition between TTSVs and signal/power TSVs imposes stringent design compromises [8], [9].

Heat sink, as a vital component of thermal management, the heat sink is typically designed with larger dimensions to provide a greater surface area for convective cooling. Conventional heat sinks face scalability challenges in 3D IC environments. Flat-plate designs suffer from thermal resistance degradation under non-uniform contact pressures caused by die warpage. Pin-fin arrays scaled for interlayer gaps (<500 μm) require pumping power >0.5 W/cm^2. Microchannel heat sinks, despite ultra-low thermal resistance, encounter flow maldistribution in vertical fluidic vias with diameters <20 μm. Copper microchannels further degrade reliability, corroding at rates of 0.2–2 nm/year in deionized water.

While extensive research has focused on optimizing these components through structural redesign, advanced materials, and novel cooling technologies, a systematic understanding of their interdependencies and holistic thermal management strategies remains elusive. This review synthesizes advancements in TIMs, TSVs, and heat sink technologies, addressing their individual limitations and collective impact on 3D IC thermal performance. Section II provides a comprehensive review of thermal interface material (TIM) design optimization. Section III delves into TSV design optimization. Section IV investigates heat sink design methodologies, with detailed analyses of three configurations: (A) flat-plate heat sinks for uniform heat dissipation, (B) pin-fin heat sinks for enhanced convective cooling, and (C) microchannel heat sinks for ultrahigh heat flux scenarios. This section further evaluates environmental factors—including ambient temperature, and humidity—on heat sink performance degradation. Section V surveys supplementary thermal management techniques to complement conventional approaches. Finally, the conclusion synthesizes critical findings, identifies unresolved challenges, and proposes future research directions for next-generation thermal solutions.

II. TIM DESIGN OPTIMIZATION

A TIM is any material that is inserted between two layers to enhance the thermal coupling and realize a low-resistance thermal contact. TIM layers are typically utilized between a heat-producing device (e.g. an integrated circuit) and a heat-dissipating device (e.g. a heat sink), as shown in Figure 2 [10]. Good thermally conductive and mechanically compliant are two basic demands for an ideal TIM, which facilitates heat transfer across the interfaces, conforms to the surface roughness, and maintains the integrity of the interface during thermomechanical stresses. However, the two demands sometimes are paradoxical, for high heat dissipation coefficient and mechanic property can't achieve both.

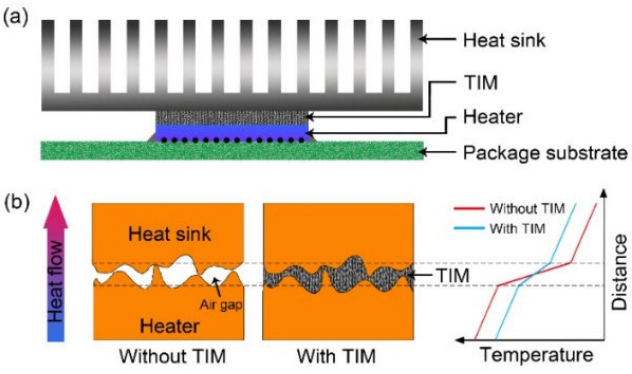

FIGURE 2. (a) Schematic diagram of a typical ball grid array electronic package (b) Schematic diagram of a TIM filling the air gap between the heater and mating interface of the heat sink.

Several researches focused on improving heat transfer performance and mechanical flexibility of TIM as shown in Figure 3a. One of the excellent solutions is to begin with an intrinsically soft material and add conductive fillers to increase the thermal conductivity as shown in Figure 3a. The intrinsically soft material can be a gel, a polymer, or a grease [11] and the conductive filler can be a graphene-polymer composite in Figure 3b, metal nanoparticles, ceramic fillers, carbon nanoparticles, and so on.

Another method is the design for mechanically compliant thermal structures, for example, building a nanostructured

conductive material (e.g., metals and graphite) into a mechanically compliant morphology, such as vertically grown nanotubes as shown in Figure 3c [12], and vertically electrodeposited nanowires in Figure 3d [13]. The thermal conductivity can be significantly enhanced by incorporating aligned arrays of continuous, conductive materials to facilitate out-of-plane heat transfer pathways. Recently, much attention has been drawn to nanostructured TIM, which is composed of vertically aligned carbon nanotubes (CNTs). Won et al. grow aligned single-walled carbon nanotube films using a micro-fabricated resonator method. The results show that factors including the zipping and unzipping of adjacent carbon nanotubes and the degree of alignment and entanglement can modulate the spatially varying local modulus, thereby fabricating CNTs with excellent mechanical and thermal properties [12], [14]. Regrettably, the thermal conductivity of the CNT array rarely exceeds 5 W/m•K. Further solutions should be investigated to solve the above problems.

Metal nanowires have excellent mechanical and thermal conduction properties which have attracted scientist's attention in the application of TIM [13], [15], [16]. The metal nanowires can be precisely designed and fabricated using templated electrodeposition to obtain excellent properties. Barako et al. [13] have integrated vertically aligned arrays of copper nanowires (CuNWs) into a soft polydimethylsiloxane (PDMS) matrix to achieve a reliable, high-performance TIM. Figure 3d shows the vertically electrodeposited copper nanowires. Thermal resistance is below 5 mm^2 K/W, over an order of magnitude lower than commercial heat sink.

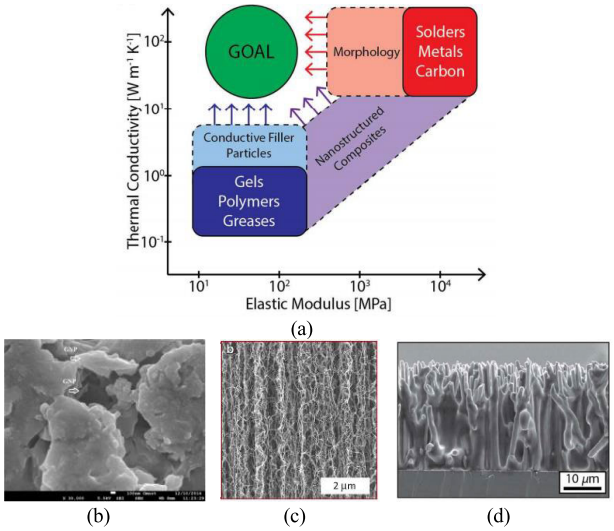

FIGURE 3. (a) Two common strategies can be employed to create high-performance TIM composites [13]; (b) an example of graphene-polymer composite [17]; (c) vertically grown nanotubes [12]; (d) vertically electrodeposited copper nanowires [13].

In addition, ultrathin graphite foams (UGFs) have aroused wide attention for their enhanced heat dissipation in the application of TIM. UGFs are usually grown via chemical vapor deposition (CVD) using sintered powder as origin templates. Evan et al. [18] grow high-thermal conductivity graphite foams on porous nickel foams template sintered by low-cost nickel powders. An effective thermal conductivity of 16.4 W/m•K has been achieved at a porosity exceeding 90 %.

Besides ultrathin graphite foams, hexagonal boron nitride (h-BN) has also been considered a promising candidate used in TIMs owing to its high thermal conductivity and excellent electrical insulation [19]. Fang et al. [20] prepared 3D-BN-ZnO scaffolds using the ice-templating method. 3D-BN-ZnO uses the excellent orientation of h-BN sheets as the main skeleton, with ZnO particles filling between h-BN sheets. This structure provides an efficient tunnel for phonon propagation which enhances heat dissipation. According to experiments, a thermal conductivity of 1.45 W/m•K has been obtained by a composition of 18.0wt% h-BN and 2.7 wt% ZnO.

Carbon fibers with ultra-high thermal conductivity and thermal stability make it an ideal choice for high-performance TIM. Li et al. [21] developed a high-performance TIM composed of carbon fiber/polydimethylsiloxane (CF/PDMS), which exhibited exceptional through-plane thermal conductivity up to 43.47 W/m•K. This remarkable performance was achieved by constructing vertically oriented carbon fiber arrays within the TIM, enabling efficient heat transfer due to the high axial thermal conductivity of carbon fibers. Additionally, the modulation of PDMS's crosslinking density resulted in outstanding elastic compliance comparable to soft biological tissues (stress∼35 kPa at 35 % compressive strain) and excellent resilience performance (resilience rate of 85 % after compression cycles). Figure 4 illustrates the application schematic of the TIM, as well as provides a depiction of the preparation process for CF/PDMS TIMs and some characterization results.

Air voids in the TIM severely prohibit the heat flow transporting from the IC device surface to the heat sink surface. Gamal et al. [22] proposed a phase-change material TIM in conjunction with a textured heat sink with multiple grooves to push the gas bubbles out of the flat surface and trapped into the groove. Because the area of flat regions is bigger than grooves, the surface-modified heat sink with a screen-printable phase-change material-based TIM has lower thermal resistance and higher heat transfer efficiency from IC die to heat sink.

Table 1 summarizes the advantages and disadvantages of different types of TIMs. Based on this comparison, by selecting advanced materials and constructing an ideal heat transfer structure, the thermal conductivity of TIM can reach a satisfactory value. However, there are still some problems to consider when developing the most advanced TIM. More attention should be paid to improving the thermal interface resistance instead of just increasing the thermal conductivity itself. Surface treatment of interface, and bonding interface quality optimization may further improve heat transfer efficiency. Moreover, further development of TIMs involves new designs with low-dimension materials, structure design, and

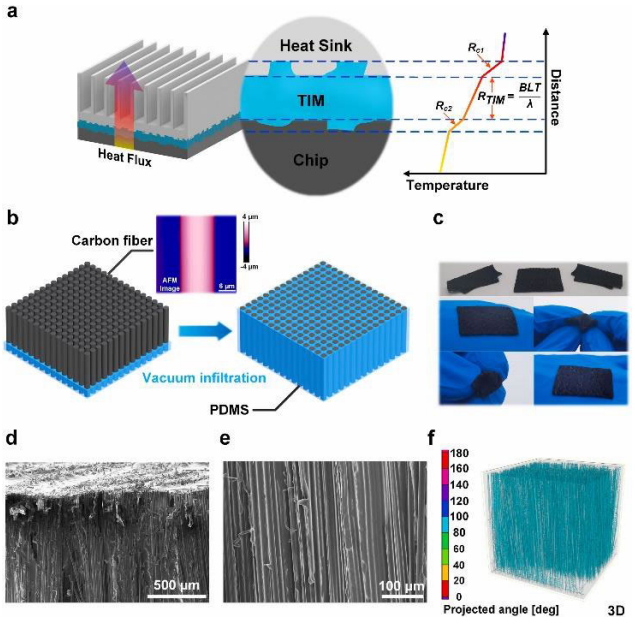

FIGURE 4. Preparation and microstructure of the CF/PDMS TIMs.(a) Schematic of TIM in the application;(b) Schematic for the preparation of the CF/PDMS TIMs; (c) Optical images of the CF/PDMS TIMs; (d–e) Microscopic morphology of the CF/PDMS TIMs; (f) Micro-CT three-dimensional structure of the CF/PDMS TIMs [21].

TABLE 1. The comparison of different types of TIMs.

Material	Thermal conductivity/Wm^{-1}K^{-1}	Mechanical compliance	Cost	Ease of fabrication
graphene-polymer composite	10-50(In plane) 1–5(Through-plane)	Excellent	High	Medium
CNT	20-150(Through-plane) [23]	Good	Hjgh	Difficult
Metal nanowires	200-400(In plane), Limited in vertical	Poor	High	Medium
UGF	500-1500(Through-plane)	Poor	High	Difficult
h-BN	5-20(Through-plane) [24]	Poor	High	Medium
Carbon fibers	10-50(Through-plane) [21]	Poor	Mediu m	Medium

optimization of fabrication methods to obtain good performance that possess additional benefits for TIM applications.

III. TSV DESIGN OPTIMIZATION

For the development of 3D integrated circuits, one of the most fundamental and critical breakthroughs is the emergence of TSV [25]. The origins of the TSV concept can be traced back to William Shockley's patent "Semiconductive Wafer and Method of Making the Same" filed in 1958. The first 3D IC stacked chips fabricated with a TSV process were invented in the 1980s in Japan [26].

In electronic engineering, a TSV is a vertical electrical connection (via) that passes completely through a silicon wafer or die. Compared to alternatives such as package-on-package, the interconnection and device density are substantially higher, and the length of the connections becomes shorter [27]. However, higher thermal resistance in the vertical direction due to the lower thermal conductivity of dielectric layers, multi-layer stacked interconnect structure, and thinned dies result in the heat generated in the devices cannot be effectively dissipated. Thus, thermal challenges are major concerns for 3D IC [1].

Optimizing the structure of TSV is an effective way to improve its thermal management performance. In terms of geometry, TSV is mainly classified into two types: cylindrical and conical. A Cylindrical TSV refers to a series of structures where the through hole is cylindrical with a circular cross-section that remains constant along its height. This category includes cylindrical TSV, coaxial TSV, annular TSV, and double annular TSV. In contrast, the through-hole of a conical TSV has a cone shape, with its radius varying in the vertical direction. Due to the limitations of the current process, only Tapered TSV is relatively common. The optimization of geometric parameters of the TSV chip is a key area of current research. For example, in his research [28], Lau adopted the heat transfer computational fluid dynamics (CFD) analysis method to conduct a comprehensive and in-depth thermal performance evaluation of the 3D stacked TSV chip filled with copper. Through detailed 3D CFD simulation, Lau investigated the influence of copper-filled TSV with different diameters, pitch, and aspect ratios on the heat conduction characteristics, and thus determined the effective thermal conductivity of the TSV chip, as shown in Figure 5. In addition, Lau's research also used correlation equations to deeply explore the effects of TSV chip stacking layer number, TSV chip thickness, heat source location, and other variables on junction temperature and thermal resistance.

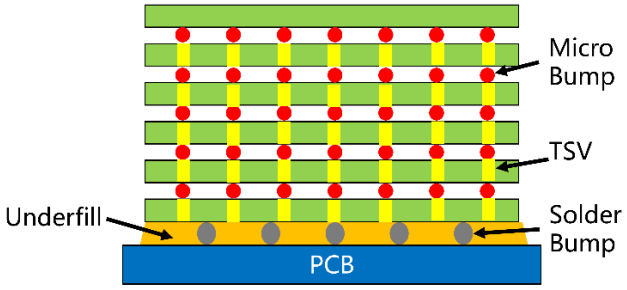

$$q = -k_{eq,z}\frac{dT}{dz} = -k_{eq,z}\frac{|\Delta T|}{\Delta z} \Rightarrow k_{eq,z} = q\frac{\Delta z}{|\Delta T|}$$
$$q = -k_{eq,x}\frac{dT}{dx} = -k_{eq,x}\frac{|\Delta T|}{\Delta x} \Rightarrow k_{eq,x} = q\frac{\Delta x}{|\Delta T|}$$
$$k_{eq,y} = k_{eq,x}$$

FIGURE 5. Equivalent thermal conductivity of TSV chips.

Cu is the traditional material for TSV. During TSV Cu electrodeposition, defects like voids and seams are usually formed, which cause both losses in thermal transport and reliability problems. To eliminate the Cu voids, Wang et al. [29] invented void-free TSV copper filling method by utilizing a triblock copolymer(ethylene oxide (EO)-propylene oxide (PO)-ethylene oxide (EO)) as a sole additive in TSV copper electrodeposition process. He has researched the impact of EO-propylene oxide-ethylene oxide (EPE) concentrations on the TSV copper plating process under various current densities. The findings revealed that lower EPE concentrations exhibited stronger inhibition capabilities for the generation of air voids and achieved ''V shape'' filling at 0.3 ASD (A/dm2). Conversely, higher EPE concentrations led to the formation of micelles within the electrolyte, resulting in decreased inhibition abilities. Furthermore, employing ultrasonic agitation during the Cu deposition process can further inhibit the air void generation enhance the TSV filling ratio, and even facilitate bottom-up filling.

Eom et al. [30] investigated the synergistic suppression effect of cetyltrimethylammonium cation (CTA^+) and bromide ion (Br^-) in copper electrodeposition for TSV filling. Electrochemical analysis revealed that CTA^+ induces negative differential resistance (NDR) enabling abrupt suppressor deactivation, while Br^- enhances surface passivation without compromising NDR characteristics. Optimal concentrations of 200 μM CTA^+ and 400 μM Br^- achieved void-free bottom-up filling in high-aspect-ratio TSVs (10 μm diameter $\times$ 60 μm depth), with excessive CTA^+ (>300 μM) causing over-passivation and surplus Br^- (>600 μM) leading to non-uniform deposition.

Other filling materials such as tungsten (W), polymer [31], solder [32], poly-Si, and carbon nanotube (CNT) [33], [34], [35] have also been reported. The implementation of W as a filling material in TSVs with diameters up to 3 mm has been demonstrated [36]. However, thick W layers deposited on wafer surfaces induce significant residual stress, leading to wafer bowing and potential interfacial delamination. To mitigate these issues, Jiao et al. [37] developed a novel hollow tungsten-filled TSV (W-TSV) structure to address thermal stress issues in high-density TSV arrays. Finite element analysis demonstrated a 60.3% reduction in thermal stress within the top 2 μm silicon substrate region, with radial stress below 20 MPa within 3 μm from the TSV interface. A CMOS-compatible process successfully fabricated ultra-high-density TSV arrays (1,600 TSVs/mm^2) featuring 640 $\times$ 512 configuration, 25 μm pitch, and 20.3 aspect ratio. Raman spectroscopy measurements confirmed maximum surface stress of 31.02 MPa, eliminating the need for keep-out zones (KOZ) around TSV arrays. In addition, a partial etch-back technique is employed, retaining a W film thickness below ~500 nm to suppress wafer deformation while preserving TSV integrity.

Compared to Cu, W exhibits closer thermal expansion coefficient (CTE) matching with Si, minimizing thermally induced stress variations and eliminating metal extrusion risks. Nevertheless, high elastic modulus (~411 GPa) and substantial intrinsic deposition stress of W exacerbate mechanical mismatch with Si substrates, constraining the maximum feasible W layer thickness.

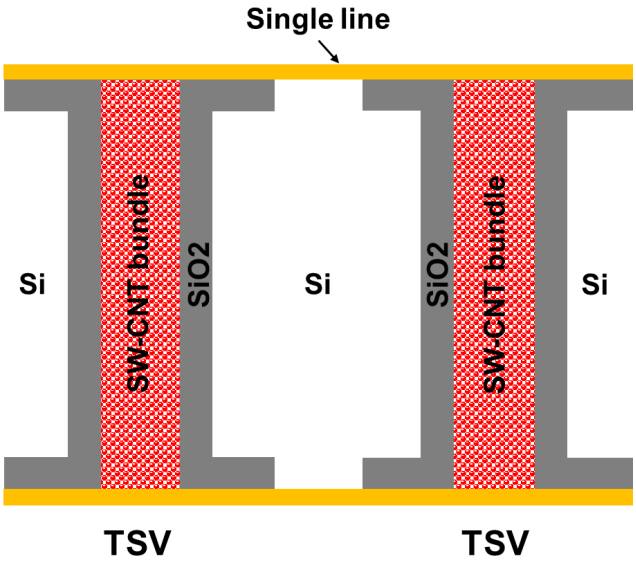

FIGURE 6. TSV filled with CNT materials.

Chan et al. [38] systematically investigated the temperature-dependent electrical characteristics of CNT TSVs. Their experimental results demonstrated that multi-walled CNTs exhibited a 45% enhancement in S21 parameter at 400 K compared to room-temperature conditions, with insertion loss reduction reaching 23% relative to conventional copper interconnects. This performance improvement was attributed to the synergistic interplay between phonon scattering mechanisms and conductive channel activation within the 300–400 K operational range, revealing MW-CNTs' superior thermal adaptability for high-density 3D integrated circuit applications. However, CNTs TSV has never materialized in commercial products of 3D IC and 2.5D packaging. Most progress in CNTs TSV focuses on numerical modeling works. Figure 6 schematically shows TSVs filled with CNT [35].

The partition design of TSV is another effective optimization strategy. The elaborate design of TSV placement can play an important role in optimizing the thermal dissipation property [39]. Hou et al. [40] proposed a novel regular triangle structure of TSV arrays to improve the thermal performance of 3D IC whereas effectively increasing the area's utilization rate of TSV. The result shows that the average temperature reduces by 0.02 % and the peak temperature reduces by 0.09 % considering the vertical heat dissipation as compared to traditional TSV cluster structure. Zhang et al. [41] investigated two types of TSV placement strategies, as depicted in Figure 7a and Figure 7b, respectively. The first type involves uniformly distributing the TSVs throughout the chip. The

second type clusters TSVs either at the center or periphery of the chip. Simulation results indicate that the maximum temperature for clustered TSVs decreases by 3.55 °C compared to the uniform distribution case. Notably, there is a remarkable drop of 6.65 °C specifically within the cell array circuits, resulting in a maximum temperature of only 42.27 °C. Consequently, by strategically clustering the TSVs away from memory cells, it can effectively isolate this thermally sensitive region from high-power components on the die surface. Kim et al. [42] proposed assignment algorithms to optimize the locations TSVs for the design of 3D ICs. Simulation results demonstrate that 3D ICs considering TSV assignment algorithms exhibit a wirelength reduction of up to 25 % compared to their 2D counterparts.

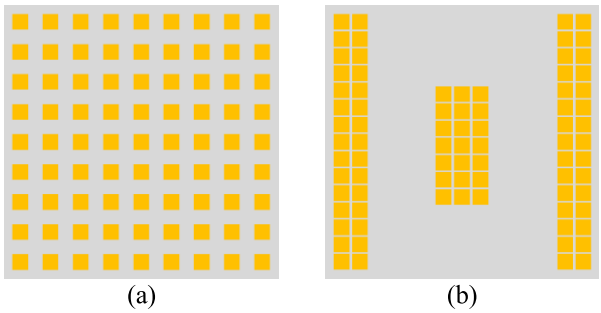

FIGURE 7. TSV distribution scenario, where the red square denotes the TSV and the thermal map (a) Uniformly distributed and (b) clustered TSVs.

Unlike conventional TSVs, TTSVs (Thermal Through-Silicon Vias) are specifically engineered for thermal management applications [43]. Singh et al. [44] studied the effects of TTSV dimensions, dielectric liner thickness, and TTSV extension length. The results show that significant cooling can be achieved by inserting a TTSV that extends across all IC layers to the substrate. Onkaraiah et al. [45] demonstrate that the temperature profile of the 3D IC stack is highly influenced by the choice of materials for the TTSV liner and conductor core, as well as TTSV dimensions. A significant cooling effect can be achieved when the liner material is a chemical vapor-deposited diamond. The thermal conductivity of CVD diamond is extremely high, up to 2000 W/m·K or more, so it can greatly improve the heat transfer efficiency and reduce the operating temperature of the chip. However, it is difficult to grow high thermal conductivity diamond materials. Furthermore, it is observed that larger diameter TTSVs exhibit enhanced temperature reduction due to their increased surface area in direct contact with Si.

To address thermal interference in 3D ICs, TSVs can be innovatively configured as thermal isolation guard rings. As illustrated in Figure 8, Hu et al. [46] demonstrated this approach by arranging TSVs in a ring-like structure around thermally sensitive components (e.g., ring oscillators), achieving efficient thermal decoupling. Simulations revealed that TSV rings (with a 10-μm diameter and SiO2 coating) exhibit thermal isolation performance comparable to metal rings, effectively mitigating heat transfer from adjacent

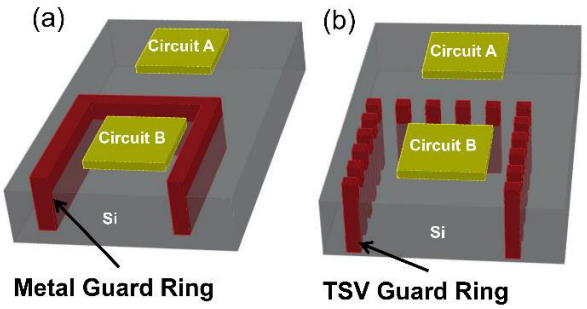

FIGURE 8. Conceptual drawings of integrating two closely located building blocks (Circuits A and B) in a chip: (a) with a metal guard ring, (b) with the TSV-based guard ring to alleviate couplings.

high-power devices. Experimental validation under localized heating showed that the frequency shift of the ring oscillator was reduced from 5.96 MHz to 2.11 MHz, while output power fluctuation decreased from 0.47 dB to 0.18 dB. Such thermal stability directly enhances energy efficiency by suppressing leakage currents (lowering static power) and preventing compensatory increases in dynamic power consumption.

IV. HEAT SINK DESIGN OPTIMIZATION

A heat sink is a passive heat exchanger used to efficiently transfer thermal energy generated by electronic or mechanical devices to a fluid medium, typically air or liquid coolant. The design of a heat sink aims to maximize its contact surface area with the surrounding cooling medium, and factors such as air velocity, material selection, protrusion design, and surface treatment can significantly impact its performance. Additionally, the attachment methods for the heat sink and the choice of thermal interface materials play crucial roles in determining the die temperature of integrated circuits. Heat sinks come in various geometries categorized into three major types: flat-plate, pin-fin, and microchannel heat sinks as shown in Figure 9. The latest research progress and optimization strategies for the three kinds of heat sinks will be reviewed in detail in the following sections.

A. FLAT-PLAT HEAT SINK

The flat plate heat sink, commonly referred to as a conventional heat sink, is extensively utilized due to its uncomplicated design and convenient manufacturability. The layout of the rectangular flat-plate heat sink is shown in Figure 10.

Many optimization methods have been proposed based on analytical investigation and experimental study. Li [47] established a correlation model between thermal resistance (R_{th}) and the Reynolds number ($R_e = \frac{\rho u L}{\mu}$, where ρ is fluid density, u is flow velocity, L is the characteristic length, and μ is dynamic viscosity) through dimensional analysis. The proposed model is expressed as:

$$R_{th} = C \cdot R_e^{-0.5} \cdot \left(\frac{H}{W}\right)^{-0.2}$$

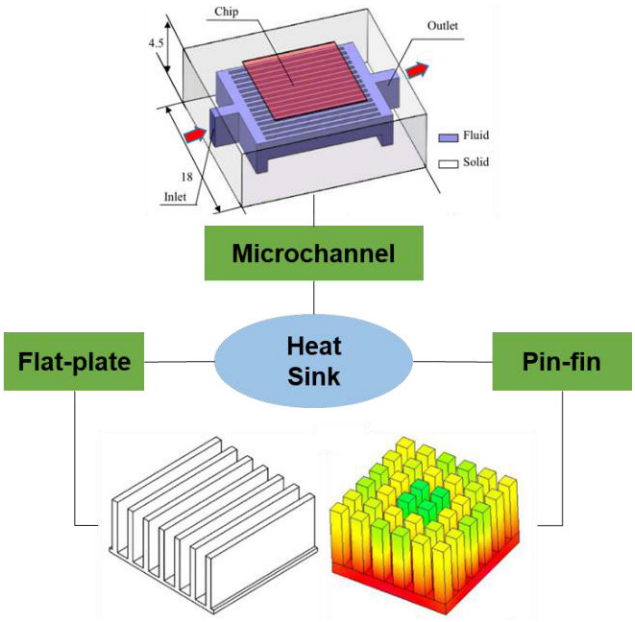

FIGURE 9. Three types of the main utilized heat sink.

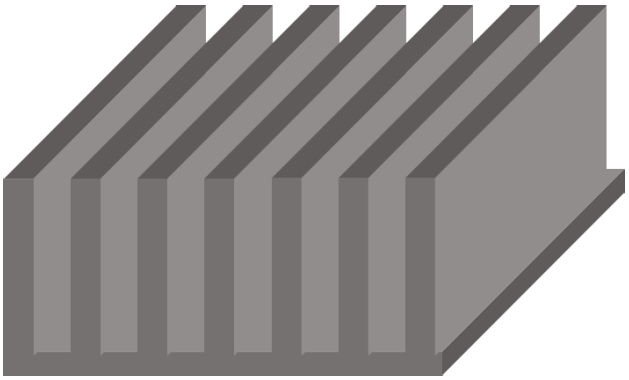

FIGURE 10. Flat-plate heat sink.

where H and W represent fin height and spacing, respectively, and C is a material-dependent constant. The experimental results show that the dimension of fins exhibited the most significant impact on thermal performance at a lower Reynolds number, which is consistent with the theoretical prediction. Morega et al. [48] demonstrated that the thermal resistance of an air-cooled heat sink can be reduced by approximately 15 % through an increase in the fin thickness along the flow direction. Kim et al. [49] developed an optimization model for natural convection heat sinks based on the volume averaging theory (VAT). They established an analytical relationship between buoyancy-driven heat transfer and flow characteristics via a modified channel Rayleigh number $R_a = g\beta\rho_f^2 c_f q''_{sf} D_h^5/\mu_f k_f^2 L$. A Nusselt number correlation $N_u = \sqrt{\frac{R_a}{16fR_e(P_{heated}/P)}}$ was derived to quantify convective performance, where f, P_{heated}, P are the friction factor, heated perimeter, total perimeter and Re is the Reynolds number. The study shows that a fin configuration with linearly thickened profiles reduces thermal resistance by up to 10% in air-cooled systems. This is achieved through variable-thickness fins that increase heat transfer surface area while maintaining favorable flow permeability, balancing buoyancy effects and viscous dissipation.

Feng et al. [50]. compared the natural convective efficiency of the conventional rectangular flat-plate heat sink and cross-fin heat sink consisting of a series of long fins and a series of perpendicularly arranged short fins as shown in Figure 11. Numerical simulations considering both natural convection and radiation heat transfer were carried out, and validated by experimental measurements. The findings revealed that the cross-fin heat sink exhibited an 11 % increase in overall heat transfer coefficient and a 15 % increase in convective heat transfer coefficient compared to the plate-fin heat sink. This performance enhancement can be primarily attributed to the improved thermo-fluidic flow pattern within the cross-fin configuration

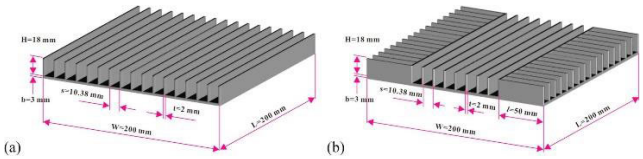

FIGURE 11. Schematic of (a) convectional plat-fin heat sink and (b) cross-fin heat sink [50].

The angle of the fins is also a crucial factor influencing the thermal performance of rectangular flat-plate heat sinks. Meng et al. [51] investigated the impact of mounting angles on heat dissipation performance under natural convection conditions. The results revealed that the performance of the heat sink reaches its peak when mounted at a 90° angle, whereas it decreases to its lowest level at a mounting angle of 15°, exhibiting a reduction of 6.88% compared to that at 90° Similarly, Sarhan et al. [52] experimentally investigated the vibration effects on the thermal performances of the rectangular flat plate under natural convection conditions in multiple angles. The experimental results illustrate that the average heat-transfer coefficient increases linearly with increasing Rayleigh number for different orientation angles. In addition, the heat transfer efficiency is highest when the plate is horizontal.

In addition to geometry optimization, adding ribs in channels of flat plate heat sinks can significantly enhance heat dissipation efficiency. Ahmed et al. [53] conducted a comprehensive analysis of rib configurations with varying sizes, positions, numbers, and orientations within the channels. Figure 12 shows the schematic diagram of the ribbed plate-fin heat sink. The concrete findings demonstrate that a ribbed plate-fin heat sink exhibits thermal performance 1.55 times greater than that of a plate-fin heat sink under corresponding conditions. Furthermore, for equivalent thermal performance, the pumping power required by the ribbed plate-fin heat sink is reduced by 69.65 % compared to its counterpart without ribs. Additionally, when considering five channels with

15 ribs, the ribbed plate-fin heat sink demonstrates hydrothermal performance 1.37 times superior to that of a nine-channel plain fin configuration.

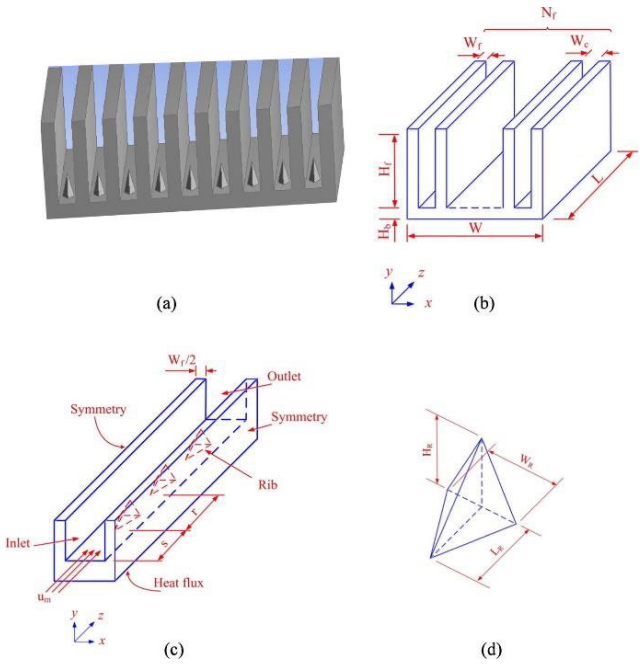

FIGURE 12. Schematic diagram of (a) ribbed plate-fin heat sink; (b) geometric parameters of plate-fin heat sink without ribs; (c) computational domain; and (d) geometric parameters of rib. The scheme is not drawn to scale [53].

A higher heat transfer enhancement was noticed by using branched fins. Kim et al. [54] conducted a comparative analysis of various fin shapes, including Y-shaped fins, inversed Y-shaped fins, and rectangular fins. Figure 13 shows the schematic of three types of heat sink. The simulation results demonstrate that the thermal resistance of the branched-fin heat sink decreases by up to 15 % [49] and 10 % [55] for water-cooled and air-cooled configurations respectively, compared to a rectangular-fin heat sink. Moreover, optimization of pumping power and length of the heat sink can lead to an additional reduction in thermal resistance by as much as 30 %.

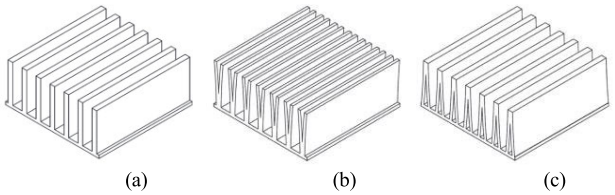

FIGURE 13. Schematic of (a) Rectangular-fin heat sink; (b) Y-shaped fin heat sink; (c) Inverted Y-shaped fin heat sink [54].

Considerable efforts have been dedicated to optimizing the design of flat plate heat sinks and enhancing their thermal performance, including optimization of fin thickness, number, and angle, as well as channel width and geometric shape. It is worth noting that not only geometry design plays a crucial role but also factors such as heat transfer type, coolant rate, and coolant type significantly impact the overall performance of the flat plate heat sink. Therefore, in the pursuit of optimal thermal performance, these factors need to be taken into account to ensure that the radiator can achieve optimal performance in different application scenarios.

B. PIN-FIN HEAT SINK

Pin fin heat sink comprises an array of pins extended from its base to increase the surface contact with the surrounding air, thus augmenting the rate of heat dissipation. The pins can be cylindrical, elliptical, or square. The shape of pin-fins is a considerable factor in heat sink efficiency enhancement. Sakanova et al. [56] quantitatively evaluate the performance differences between pin-fin radiators (round, conical, hydrofoil) and finned radiators by using Nu, Re and thermal performance index (η), where $N_u = hD_h/k$, $\eta = \frac{N_u/N_{u0P}}{(f/f_{0P})^3}$. The diagram of the circular, cone, and hydrofoil fin is shown in Figure 14. The findings indicate that among the three types of pin-fin heat sinks, the cone-shaped design exhibits the highest heat transfer coefficient. This can be attributed to the flow separation effect induced by the pin-fins, which significantly increased Nussel number and promotes efficient heat transfer. Moreover, compared to traditional finned configurations, pin-fin heat sinks demonstrate superior thermal performance by 1.6-2 times. Additionally, utilizing pin-fin shapes can reduce up to half of the weight typically associated with conventional finned heat sinks. Hua [57] presents an experimental study investigating the heat transfer characteristics of various micro pin fin shapes, including circular, ellipse, diamond, square, and triangle arrays. The study examines the influence of different sizes and shapes of pin fins on Nusselt number and heat transfer coefficient. It is observed that increasing the Nusselt number leads to an enhancement in the convective heat transfer coefficient. Notably, among all the investigated pin fin shapes, the ellipse shape exhibits superior heat transfer performance.

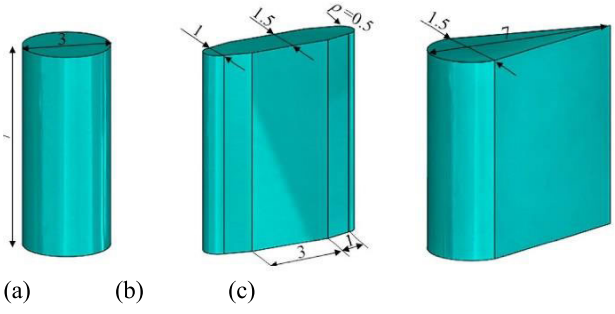

FIGURE 14. The diagram of (a) circular pin-fin; (b) hydrofoil pin-fin; (c) cone pin-fin [56].

To deliver better heat transfer and fluid flow characteristics, fin height as an important factor has been extensively conducted. According to Bhandari et al., [58] pin fin height

affects the heat transfer performance because of Dean vortices formation. The study reported that the enhancement of heat transfer performance in the microchannel with a fin height of 1.5 mm was higher when compared with a fin height of 2.0 mm, which is attributed to net convective surface area and availability of the open space that facilitates favorable flow behavior for better heat transfer.

The optimization of pin-fin heat sinks extends beyond geometry and physical shape considerations, as the direction of pin-fins can significantly impact their thermal performance. In an experimental study conducted by Huang et al. [59] experimentally investigated the natural convective performance of square pin fin heat sinks under different orientations (upward, sideward, downward). A mathematical framework integrating the Rayleigh number $R_a = g\beta\,(T_b - T_a)\,L^3/\nu\alpha$ and finning factor which represents the total surface area divided by the base surface area revealed distinct heat transfer behaviors. The downward orientation exhibited the lowest Nu due to restricted buoyancy-driven flow. Sideward arrangement outperforms the upward one for small finning factors below 2.7, beyond which the situation is reversed due to flow blockage in sideward channels. These findings provide valuable insights into the design and optimization of heat sinks in various applications involving natural convection cooling mechanisms.

Several studies have considered the effect of perforations of pin fin heat sinks on heat transfer and pressure drops. Al-Sallami et al. [60] conducted a comparative analysis of staggered and in-line arrangements of strip fins, with cross-sectional aspect ratios falling between those for plate fins (high aspect ratio) and pin fins (aspect ratio ≈ 1). Heat sinks with solid and perforated fins in in-line or staggered arrangements are shown in Figure 15. The findings demonstrate that strip fins offer an effective approach to enhancing heat transfer, particularly when implemented in staggered arrangements. Furthermore, numerical investigations reveal that incorporating perforations into the strip fins yields additional improvements in terms of enhanced heat transfer, reduced pressure loss, and decreased heat sink mass.

Furthermore, the dimensions and configurations of cavities and holes within the pin-finned heat sink represent a significant variable that should be considered as a crucial factor in thermal performance analysis. Al-Damook et al. [61] conducted a simulation of a pin-fin heat sink featuring a rectangular slotted or notched hole. The results demonstrate that the utilization of rectangular perforation leads to an enhancement in heat transfer and a reduction in fan power, as compared to the corresponding pin-fin heat sink with solid pins. Moreover, it is observed that both the rate of heat transfer and fan power exhibit a consistent increase as the size of the perforation expands. Notably, the largest slotted and notched perforations investigated have exhibited an ability to elevate the heat transfer rate by more than 10 %, whereas concurrently reducing fan power consumption and pin weight by over 30 % and 40 % respectively. Hajmohammadi et al. [62] introduced a novel tree-shaped pattern for the cavity

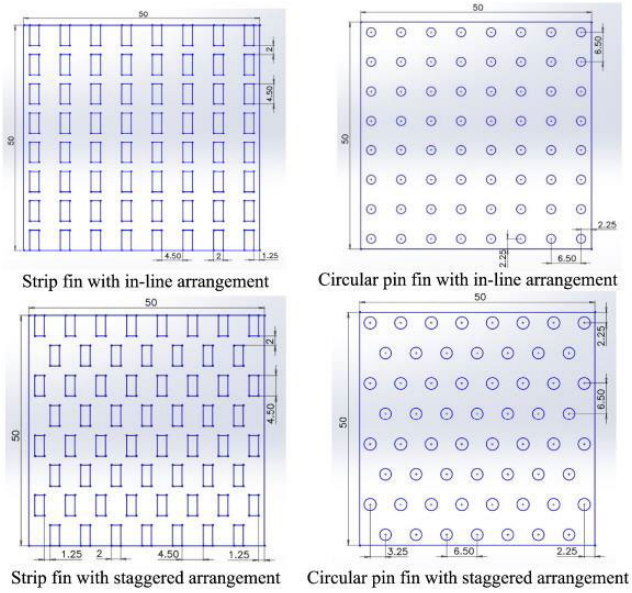

FIGURE 15. Schematic diagram of different heat sink geometries and arrangements [60].

structure of a pin-finned heat sink, aiming to optimize its thermal performance. The experimental findings demonstrated that the maximum excess temperature obtained in the final configuration with four branches was approximately 50 % lower compared to the most optimal design reported in existing literature.

C. MICROCHANNEL HEAT SINK

Microchannels, characterized by a hydraulic diameter below 1mm and typically ranging from 1 to 99 μm, find extensive applications in fluid control and heat transfer. The pioneering work on microchannel design was introduced by Tuckerman and Pease of Stanford Electronics Laboratories in 1981, who conducted experimental investigations on the performance of microchannels. The results demonstrate that straight microchannel heat sinks exhibit superior performance in terms of heat flux removal, with capabilities up to 790 W/cm^2. However, it should be noted that the high-pressure drop associated with microchannels poses limitations on their overall performance.

Extensive experimental and numerical investigations have been conducted to explore the impact of geometric parameters on enhancing heat transfer in microchannel heat sinks [63], [64]. Tan et al. [65] employed fluid-thermal coupling numerical simulations to compare the thermal performance of five topological microchannel structures (ternate veiny, lateral veiny, snowflake-shaped, spider-netted, and honeycomb-shaped). Figure 16 shows the temperature contours on chips of all microchannel topologies. Results demonstrated that the spider-netted microchannel exhibited optimal heat dissipation under 100 W/cm^2 heat flux, achieving a maximum temperature reduction of 9.9°C compared to straight channels. The enhanced performance was attributed

to topology-driven modulation of flow patterns and heat transfer area, which synergistically optimized the Nu and Re correlations. While straight channels exhibited limited Nu due to fully developed laminar flow, the spider-netted structure enhanced secondary flow disturbances and expanded effective heat transfer area, significantly elevating Nu. Hence, according to numerical and experimental results, it can be concluded that the significant influence of microchannel topology on heat transfer efficiency, particularly under high heat flux conditions.

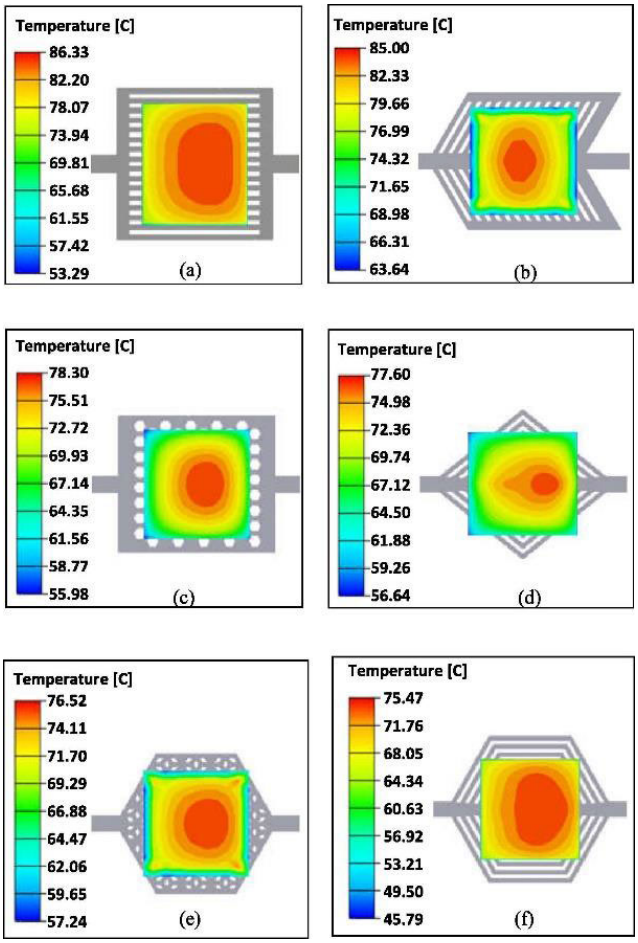

FIGURE 16. Temperature contours of the chip. (a) Straight microchannel; (b) lateral veiny microchannel; (c) honeycomb-shaped microchannel; (d) ternate veiny microchannel; (e) snowflake-shaped microchannel; (f) spider netted microchannel [65].

In the research [66], an experimental and numerical investigation into the thermal-hydraulic transport characteristics of various complex grooves for utilization in a water-cooled heat sink was conducted. The grooves show higher heat transfer coefficients and pressure drops compared to the straight geometry, with increments of up to 2.25 and 8.54 times, respectively. This can be attributed to the expansion of the flow path as well as the generation of swirling flows within the intricate grooves. Figure 17 shows the temperature contour of different groove models at a Reynolds number of 1000.

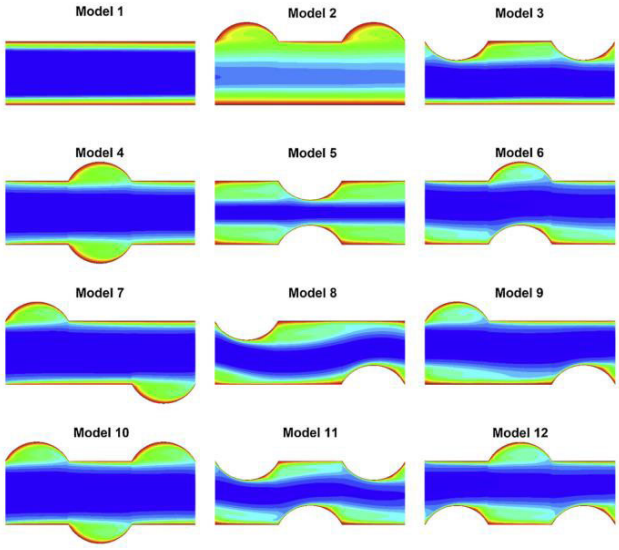

FIGURE 17. A part of the temperature contour of different models on the x–y plane at Re = 1000 [66].

Chai et al. [67] systematically analyzed the thermohydraulic performance of microchannel heat sinks with triangular ribs on sidewalls through a three-dimensional conjugate heat transfer model accounting for temperature-dependent fluid properties and viscous heating. Key geometric parameters, rib-to-channel width ratio (Wr/Wc)), height ratio (Hr/Wc), spacing ratio (Sr/Wc), and converging ratio (Wcon/Wr), as well as rib arrangements (aligned or offset) were investigated. The geometric parameters of triangular ribs are shown in Figure 18. Results demonstrated that the offset arrangement enhanced cold-hot fluid mixing via secondary flow, achieving an average Nusselt number 2.15 times higher than the straight microchannel at Re = 443. However, the aligned arrangement exhibited higher friction factors due to converging-diverging flow passage effects. Optimized rib height (Hr/Wc > 0.15) and reduced spacing (Sr/Wc = 2.5) significantly improved Nu, with a 50% reduction in substrate temperature rise at Hr/Wc = 0.25. Smaller rib spacing (Sr/Wc = 2.5) suppressed the decay of Nu along the flow direction through periodic boundary-layer redevelopment. The comprehensive performance metric $Nu/f^{1/3}$ revealed that the offset configuration with minimal spacing (0.25 mm) delivered optimal thermal enhancement, primarily attributed to intensified fluid mixing and boundary-layer disruption. In his recent research [68], the study proposes correlations between the average friction factor and Nusselt number. The microchannel heat sinks with aligned triangular ribs exhibit an increase of 1.03–2.01 times in the average Nusselt number and a rise of 1.06–9.09 times in the average friction factor compared to the typical straight microchannel heat sink. The authors [69] also analyzed the impact of various rib configurations, such as rectangular, backward triangular, diamond, forward triangular, and ellipsoidal shapes, on thermal-hydraulic performance. Their findings revealed

that interrupted microchannel heat sink with ribs in the transverse microchambers exhibited a reduction of 4-26 % in entropy generation and a decline of 4-31 % in thermal resistance. Furthermore, it was observed that the thermal performance improved by approximately 1.39 time.

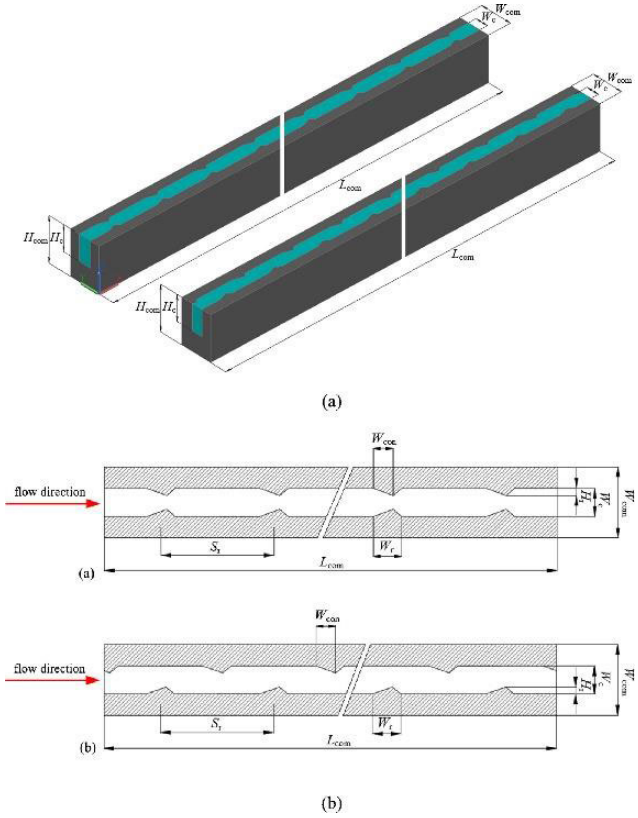

FIGURE 18. Microchannel heat sinks with triangular ribs on sidewalls for (a) aligned arrangements; (b) offset arrangements [67].

A comprehensive review has been presented by Lee et al. [70], indicating that the combination of various individual techniques can effectively enhance the heat transfer coefficient. The incorporation of ribs and cavities represents a highly effective approach for enhancing the heat transfer performance of microchannel heat sinks. Xia et al. [71] have investigated the impact of triangular reentrant cavities on heat transfer characteristics. The enhancement in heat transfer can be attributed to both the formation of vortices within the reentrant cavity, leading to chaotic advection and convective fluid mixing, as well as the periodic interruption and redevelopment of thermal boundary layers along the constant cross-section surface. The combination of a cavity and rib has also been subjected to numerical investigation by Japer et al. [72]. The study compared various configurations of ribs and cavities within a microchannel, including a microchannel with a triangular cavity, rectangular rib, and secondary channel design (TC-RR-SC), a microchannel with only rectangular rib (CR-RR), a microchannel with only a triangular cavity (TC), and finally, a microchannel featuring both rectangular rib and triangular cavity (TC-RR) as shown in Figure 19. The results demonstrate that the proposed TC-RR-SC design exhibits exceptional overall performance when compared to other designs due to its combined effect on thermal boundary layer re-development and flow mixing in the main channel. Similar research has been conducted by Ghani et al. [73] and Li et al. [74].

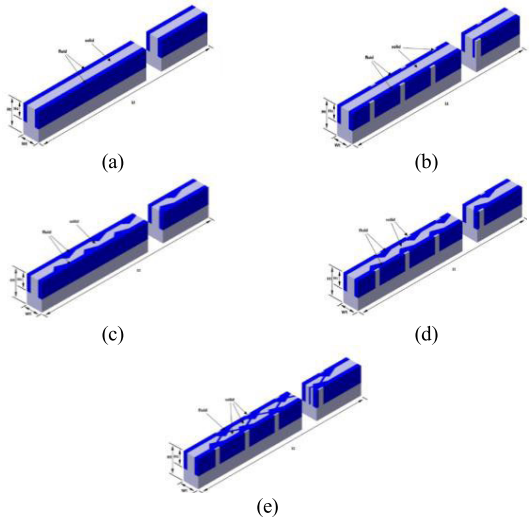

FIGURE 19. Schematic of microchannel of (a) Conventional rectangular microchannel heat sink (CR MCHS); (b) Conventional rectangular and rectangular ribs (CR-RR MCHS); (c) Triangular cavities(TC MCHS); (d) Triangular cavities and rectangular ribs(TC-RR MCHS); (e) Triangular cavities, rectangular ribs and secondary channel (TCRR-SC MCHS) [72].

Bayrak et al. [75]. compared the impact of five different geometric structures of microchannel heat sinks on flow characteristics and heat transfer performance. The presence of cavities and ribs in MCHS leads to enhanced heat transfer performance compared to configurations without them, primarily due to localized modifications within the channels that ensure suitable fluid mixing between the core flow and near-wall regions. However, for the asymmetrical cavity and rib configuration, this effect is reversed due to the formation of intense recirculation zones. The results indicate that the symmetrical cavity and rib exhibit superior thermal performance whereas the asymmetrical cavity demonstrates optimal uniform temperature distribution along the baseline wall The study demonstrates that the formation of vortices in a cavity is important for enhancing heat transfer as it ensures mixing between cold and hot water streams. However, inappropriate design of the cavity can lead to the amplification of recirculation zones, which hinder heat transfer between near walls and core flow, resulting in localized regions with elevated temperatures.

The characteristics of flow in microchannels and microtubes have also attracted much attention from researchers [76], [77]. The nanofluid is an important and attractive heat transport fluid because the presence of nanoparticles in the base fluid has increased the heat transfer coefficient of the base fluid due to the thermal conductivity of solid particles being higher than fluid. Jiang et al. [78] investigated

the cooling performance of a microchannel heat sink with nanofluids numerically. The findings indicate that the cooling performance of a microchannel heat sink employing water-based nanofluids containing diamond, under a constant pumping power of 2.25 W, is approximately 10 % superior to that of a microchannel heat sink utilizing water alone. The heat transfer enhancement effect of a system utilizing an Al_2O_3/water nanofluid-cooled MCHS was investigated by Hung [79]. The study demonstrated a significant improvement in heat transfer performance, with a remarkable increase of 21.6 % observed when employing Al_2O_3-water and diamond-water nanofluids compared to pure water. These findings highlight the potential for enhanced heat transfer capabilities offered by these nanofluids, as supported by the research conducted.

D. ENVIRONMENTAL FACTORS

Environmental factors, including ambient temperature, humidity, and air pressure, critically influence heat sink performance in practical applications.

Çorumlu [80] systematically investigated the role of ambient temperature on natural convection dynamics. At a moderate input power of 16.5 W, increasing ambient temperature from 30 ° to 40 ° improved convective heat transfer coefficients (h: 30.45 →31.31 W/m^2·K) and Nusselt numbers (Nu: 21.94 →22.20), indicating enhanced convective cooling efficiency. However, under high-power conditions (33 W), while h continued to rise (31.85 → 32.17 W/m^2·K), Nu exhibited a slight decline (21.73→21.61), suggesting diminished dimensionless heat transfer efficiency due to intensified thermal boundary layer resistance. Additionally, thermal resistance (Rth) decreased with rising ambient temperature (2.93 → 2.75 K/W), reflecting improved overall heat dissipation. These results highlight the dual role of ambient temperature: it enhances convective cooling at lower power but introduces efficiency trade-offs under high thermal loads.

In contrast, Kope et al. [81] explored the impact of air humidity on the efficiency of the radiator, proposing an innovative approach using ultrasonic water vapor to amplify natural convection. Their experiments demonstrated that saturating air with water vapor enabled a 35 % increase in transistor power dissipation (from 22 W to 31 W) while maintaining a junction temperature of 150 °C. This is because water vapor takes more heat from the heat sink and hence cools it better allowing for higher power dissipation in the transistor. Notably, this method addresses limitations of passive cooling in high-humidity environments, offering a scalable solution for power-dense electronics.

Collectively, these studies underscore the nuanced interplay between environmental factors and thermal management. While elevated temperatures may improve heat sink performance under moderate loads, high-power scenarios necessitate careful optimization to mitigate efficiency losses. Furthermore, humidity modulation via active methods like ultrasonic vapor injection presents a promising avenue to overcome inherent limitations of natural convection, particularly in thermally constrained systems.

V. OTHER THERMAL DESIGN

Carbon-based materials are good options for TIM, TSV, and heat sinks due to their low density and relatively high thermal conductivity. Graphene has been used as TTSV material, of which the thermal properties have been explored by simulation. The results showed that graphene-based fin and spreader structure exhibit better performance compared to CNT in terms of noise coupling, whereas CNT-based structure is thermally superior to Graphene. Unfortunately, no experimental work was reported [82]. More work is needed to verify the relevant theories in the future. Other research concerning graphene used as a heat spreader and TIM has also been reported. Barua et al. [83] have studied the effect of graphene heat spreaders in the thermal management of 3D chips, the simulation results showed that the maximum temperature can be reduced with graphene heat spreaders. K.Vendra et al. [84] compared the impact of Graphene-based TIM and Graphit-based TIM on the peak temperature of 3D IC, proving that although graphene has an outstanding thermal conductivity of 3000-5000 W/m K, the lower thickness of Graphene will hamper the heat dissipation.

Moreover, a hybrid approach combining interlayer with microfluidic cooling has been investigated. By embedding microchannels into the silicon interposer, the number of thermal interface materials can be significantly reduced but requires sealed fluid interconnects from the system fluid loop to the silicon chip stack [85]. Oh et al. [86] conducted microfluidic cooling experiments using the fabricated test equipment, verifying experimentally the effectiveness of interposer along with microfluidic cooling technology in terms of thermal isolation between layers. Figure 20 shows the conventional air-cooled heat sink and the proposed 3D system featuring microfluidic cooling embedded within an interposer package. Furthermore, it reported high-aspect-ratio (23:1) TSVs to enable their integration within the microfluidic heat sink and preserve the electrical benefits.

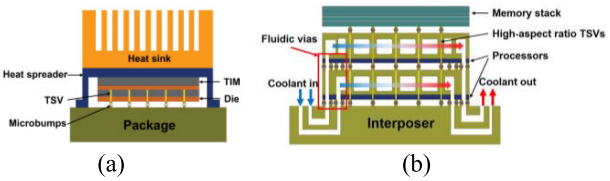

FIGURE 20. Schematics of (a) conventional air-cooled heat sink; and (b) the proposed 3D system featuring microfluidic cooling embedded within an interposer package, high-aspect-ratio TSVs, and micro bumps for electrical I/Os.

VI. CONCLUSION

In this paper, a comprehensive and systematic study of the critical thermal problems in the 3D ICs is presented. The key developments in heat transfer in TIM, TSV, and heat sink from pertinent literature were summarized, and the effects

of various significant parameters, such as TIM thermal conductivity, TSV geometry characteristics, TSV arrangements, materials variation, shape variation as well as the geometry and shape parameters of heat sinks are analyzed in detail.

The research on TIMs involves the introduction of high conductive fillers and the design of mechanically compliant thermal conductors, including carbon nanotubes, metal nanowires, ultrathin graphite foams, porous foam architectures of hexagonal BN, and carbon fibers.

TSVs are central to 3DIC integration. Various methods, such as geometric parameters adjustment, dielectric layer optimization, and the introduction of new materials, have been adopted by researchers for the reduction of thermal issues in 3D structures. Additionally, careful selection and placement of TSV materials are essential for enhancing thermal conductivity.

Different from TIM and TSV, a heat sink functions as a passive heat exchanger that facilitates the transfer of thermal energy across various geometries categorized primarily into flat-plate, pin-fin, and microchannel types. The fin height, width, number, fin orientation, and fin shape can significantly impact thermal properties. Considering these factors simultaneously can optimize thermal efficiency. Additionally, some structure designs, including cross-fin, branched fin, cavities and holes, are considered critical variables in improving thermal performance. Flat-plate and Pin-fins offer great thermal performance for heat sinks, but they may be merged with other types of heat sinks such as microchannels. A microchannel heat sink provides a very good thermal reduction performance. Not only microchannel topologies but also some special structures in heat sinks, such as grooves, ribs, and the combination of cavities and ribs, can affect thermal performance.

Despite considerable attention from the electronic packaging community towards various thermal management techniques, traditional methods are usually limited to a single design scale, such as device thermal management, package thermal management, or system thermal management. Many previous solution techniques operate in isolation and may eventually conflict with each other. Therefore, it is necessary to conduct collaborative optimization of the key structures in three-dimensional integrated circuits to solve the hot spot problem to the greatest extent. It is expected that the summary of the current state-of-the-art thermal technologies in 3D ICs will help researchers in both academic and industry who are addressing these and related challenges.

REFERENCES

[1] V. Venkatadri, B. Sammakia, K. Srihari, and D. Santos, "A review of recent advances in thermal management in three dimensional chip stacks in electronic systems," *J. Electron. Packag.*, vol. 133, no. 4, Dec. 2011, Art. no. 041011, doi: 10.1115/1.4005298.

[2] J. C. Kim, Z. Ren, A. Yuksel, E. M. Dede, P. R. Bandaru, D. Oh, and J. Lee, "Recent advances in thermal metamaterials and their future applications for electronics packaging," *J. Electron. Packag.*, vol. 143, no. 1, Mar. 2021, Art. no. 010801, doi: 10.1115/1.4047414.

[3] H. Yu, L. Li, and Y. Zhang, "Silver nanoparticle-based thermal interface materials with ultra-low thermal resistance for power electronics applications," *Scripta Mater.*, vol. 66, no. 11, pp. 931–934, Jun. 2012, doi: 10.1016/j.scriptamat.2012.02.037.

[4] J. D. Renteria, S. Ramirez, H. Malekpour, B. Alonso, A. Centeno, A. Zurutuza, A. I. Cocemasov, D. L. Nika, and A. A. Balandin, "Strongly anisotropic thermal conductivity of free-standing reduced graphene oxide films annealed at high temperature," *Adv. Funct. Mater.*, vol. 25, no. 29, pp. 4664–4672, Aug. 2015, doi: 10.1002/adfm.201501429.

[5] H.-H. Chen, Y. Zhao, and C.-L. Chen, "Experimental study of coefficient of thermal expansion of aligned graphite thermal interface materials," *Frontiers Heat Mass Transf.*, vol. 4, no. 1, pp. 1–7, May 2013, doi: 10.5098/hmt.v4.1.3004.

[6] F. Wu, W. Cui, J. Zhao, Q. Zhang, H. Li, H. Zhang, and J. Shen, "Fabrication of high aspect ratio TSV interposer with cu-cu direct bonding," in *Proc. 25th Int. Conf. Electron. Packag. Technol. (ICEPT)*, Tianjin, China, Aug. 2024, pp. 1–4, doi: 10.1109/ICEPT63120.2024.10668458.

[7] Q. Xu and S. Chen, "Fast thermal analysis for fixed-outline 3D floorplanning," *Integration*, vol. 59, pp. 157–167, Sep. 2017, doi: 10.1016/j.vlsi.2017.06.013.

[8] V. Kiran Sanipini, B. Rakesh, A. Jyothi Chamanthula, N. Santoshi, A. Arunkumar Gudivada, and A. Kumar Panigrahy, "Thermal management in TSV based 3D IC integration: A survey," *Mater. Today, Proc.*, vol. 45, pp. 1742–1746, Jan. 2021, doi: 10.1016/j.matpr.2020.08.621.

[9] Z. Ren, A. Alqahtani, N. Bagherzadeh, and J. Lee, "Thermal TSV optimization and hierarchical floorplanning for 3-D integrated circuits," *IEEE Trans. Compon., Packag., Manuf. Technol.*, vol. 10, no. 4, pp. 599–610, Apr. 2020, doi: 10.1109/TCPMT.2020.2970382.

[10] L. Lv, W. Dai, J. Yu, N. Jiang, and C.-T. Lin, "A mini review: Application of graphene paper in thermal interface materials," *New Carbon Mater.*, vol. 36, no. 5, pp. 930–938, Oct. 2021, doi: 10.1016/s1872-5805(21)60093-8.

[11] C. I. Idumah and A. Hassan, "Recently emerging trends in thermal conductivity of polymer nanocomposites," *Rev. Chem. Eng.*, vol. 32, no. 4, pp. 413–457, Jan. 2016, doi: 10.1515/revce-2016-0004.

[12] Y. Won, Y. Gao, M. A. Panzer, S. Dogbe, L. Pan, T. W. Kenny, and K. E. Goodson, "Mechanical characterization of aligned multi-walled carbon nanotube films using microfabricated resonators," *Carbon*, vol. 50, no. 2, pp. 347–355, Feb. 2012, doi: 10.1016/j.carbon.2011.08.009.

[13] M. T. Barako, S. G. Isaacson, F. Lian, E. Pop, R. H. Dauskardt, K. E. Goodson, and J. Tice, "Dense vertically aligned copper nanowire composites as high performance thermal interface materials," *ACS Appl. Mater. Interface*, vol. 9, no. 48, pp. 42067–42074, Dec. 2017, doi: 10.1021/acsami.7b12313.

[14] Y. Won, Y. Gao, M. A. Panzer, R. Xiang, S. Maruyama, T. W. Kenny, W. Cai, and K. E. Goodson, "Zipping, entanglement, and the elastic modulus of aligned single-walled carbon nanotube films," *Proc. Nat. Acad. Sci. USA*, vol. 110, no. 51, pp. 20426–20430, Dec. 2013, doi: 10.1073/pnas.1312253110.

[15] M. T. Barako, S. Roy-Panzer, T. S. English, T. Kodama, M. Asheghi, T. W. Kenny, and K. E. Goodson, "Thermal conduction in vertically aligned copper nanowire arrays and composites," *ACS Appl. Mater. Interface*, vol. 7, no. 34, pp. 19251–19259, Sep. 2015, doi: 10.1021/acsami.5b05147.

[16] A. Bar-Cohen, K. Matin, and S. Narumanchi, "Nanothermal interface materials: Technology review and recent results," *J. Electron. Packag.*, vol. 137, no. 4, Dec. 2015, Art. no. 040803, doi: 10.1115/1.4031602.

[17] M.-T. Le and S.-C. Huang, "Thermal and mechanical behavior of hybrid polymer nanocomposite reinforced with graphene nanoplatelets," *Materials*, vol. 8, no. 8, pp. 5526–5536, Aug. 2015, doi: 10.3390/ma8085262.

[18] E. Fleming, I. Kholmanov, and L. Shi, "Enhanced specific surface area and thermal conductivity in ultrathin graphite foams grown by chemical vapor deposition on sintered nickel powder templates," *Carbon*, vol. 136, pp. 380–386, Sep. 2018, doi: 10.1016/j.carbon.2018.04.082.

[19] D. An, S. Cheng, Z. Zhang, C. Jiang, H. Fang, J. Li, Y. Liu, and C.-P. Wong, "A polymer-based thermal management material with enhanced thermal conductivity by introducing three-dimensional networks and covalent bond connections," *Carbon*, vol. 155, pp. 258–267, Dec. 2019, doi: 10.1016/j.carbon.2019.08.072.

[20] H. Fang, A. Chen, L. Zhang, S. Chen, F. Wu, and H. Chen, "Synergistic enhancement of thermal conductivity in thermal interface materials by fabricating 3D-BN-ZnO scaffolds," *Polym. Eng. Sci.*, vol. 62, no. 5, pp. 1641–1649, May 2022, doi: 10.1002/pen.25952.

[21] J. Li, Z. Ye, P. Mo, Y. Pang, E. Gao, C. Zhang, G. Du, R. Sun, and X. Zeng, "Compliance-tunable thermal interface materials based on vertically oriented carbon fiber arrays for high-performance thermal management," *Composites Sci. Technol.*, vol. 234, Mar. 2023, Art. no. 109948, doi: 10.1016/j.compscitech.2023.109948.

[22] G. Refai-Ahmed, H. Do, B. Philofsky, and J. Strader, "Extending the performance of high heat flux 2.5D and 3D packaging from component-system interaction," in *Proc. 19th Int. Conf. Thermal, Mech. Multi-Phys. Simulation Exp. Microelectron. Microsyst. (EuroSimE)*, Apr. 2018, pp. 1–6, doi: 10.1109/EUROSIME.2018.8369893.

[23] R. Bahru and M. A. Mohamed, "Enhancement of thermal interface material properties using carbon nanotubes through simple electrophoretic deposition method," *Int. J. Energy Res.*, vol. 44, no. 6, pp. 4944–4960, May 2020, doi: 10.1002/er.5221.

[24] Q. Hu, X. Bai, C. Zhang, X. Zeng, Z. Huang, J. Li, J. Li, and Y. Zhang, "Oriented BN/silicone rubber composite thermal interface materials with high out-of-plane thermal conductivity and flexibility," *Compos. A, Appl. Sci. Manuf.*, vol. 152, Jan. 2022, Art. no. 106681, doi: 10.1016/j.compositesa.2021.106681.

[25] J. Wang, F. Duan, Z. Lv, S. Chen, X. Yang, H. Chen, and J. Liu, "A short review of through-silicon via (TSV) interconnects: Metrology and analysis," *Appl. Sci.*, vol. 13, no. 14, p. 8301, Jul. 2023, doi: 10.3390/app13148301.

[26] J. H. Lau, "Evolution, challenge, and outlook of TSV, 3D IC integration and 3D silicon integration," in *Proc. Int. Symp. Adv. Packag. Mater. (APM)*, Oct. 2011, pp. 462–488, doi: 10.1109/ISAPM.2011.6105753.

[27] P.-Y. Hsu, H.-T. Chen, and T. Hwang, "Stacking signal TSV for thermal dissipation in global routing for 3-D IC," *IEEE Trans. Comput.-Aided Design Integr. Circuits Syst.*, vol. 33, no. 7, pp. 1031–1042, Jul. 2014, doi: 10.1109/TCAD.2014.2307488.

[28] J. H. Lau and T. G. Yue, "Thermal management of 3D IC integration with TSV (through silicon via)," in *Proc. 59th Electron. Compon. Technol. Conf.*, San Diego, CA, USA, May 2009, pp. 635–640, doi: 10.1109/ECTC.2009.5074080.

[29] F. Wang, Y. Tian, K. Zhou, R. Yang, T. Tan, Y. Wang, and W. Yao, "Using a triblock copolymer as a single additive in high aspect ratio through silicon via (TSV) copper filling," *Microelectron. Eng.*, vols. 244–246, May 2021, Art. no. 111554, doi: 10.1016/j.mee.2021.111554.

[30] H. W. Eom, H. Kwak, C.-M. Yang, W. Y. Lee, M. H. Lee, and M. J. Kim, "Synergistic effect of CTA+ and Br- on defect-free TSV filling by Cu electrodeposition," *Electrochimica Acta*, vol. 503, Nov. 2024, Art. no. 144879, doi: 10.1016/j.electacta.2024.144879.

[31] M. Bouchoucha, P. Chausse, S. Moreau, L-L. Chapelon, N. Sillon, and O. Thomas, "Reliability study of 3D-WLP through silicon via with innovative polymer filling integration," in *Proc. IEEE 61st Electron. Compon. Technol. Conf. (ECTC)*, Lake Buena Vista, FL, USA, May 2011, pp. 567–572, doi: 10.1109/ECTC.2011.5898568.

[32] Y.-K. Ko, H. T. Fujii, Y. S. Sato, C.-W. Lee, and S. Yoo, "Advanced solder TSV filling technology developed with vacuum and wave soldering," in *Proc. IEEE 61st Electron. Compon. Technol. Conf. (ECTC)*, Lake Buena Vista, FL, USA, May 2011, pp. 2091–2095, doi: 10.1109/ECTC.2011.5898806.

[33] A. Gupta, S. Kannan, B. C. Kim, F. Mohammed, and B. Ahn, "Development of novel carbon nanotube TSV technology," in *Proc. 60th Electron. Compon. Technol. Conf. (ECTC)*, Las Vegas, NV, USA, Jun. 2010, pp. 1699–1702, doi: 10.1109/ECTC.2010.5490749.

[34] S. Kannan, A. Gupta, B. C. Kim, F. Mohammed, and B. Ahn, "Analysis of carbon nanotube based through silicon vias," in *Proc. 60th Electron. Compon. Technol. Conf. (ECTC)*, Las Vegas, NV, USA, Jun. 2010, pp. 51–57, doi: 10.1109/ECTC.2010.5490885.

[35] M. F. Abdullah and H. W. Lee, "Technology review of CNTs TSV in 3D IC and 2.5D packaging: Progress and challenges from an electrical viewpoint," *Microelectronic Eng.*, vol. 290, Jul. 2024, Art. no. 112189, doi: 10.1016/j.mee.2024.112189.

[36] F. Liu, R. R. Yu, A. M. Young, J. P. Doyle, X. Wang, L. Shi, K. N. Chen, X. Li, D. A. Dipaola, D. Brown, C. T. Ryan, J. A. Hagan, K. H. Wong, M. Lu, X. Gu, N. R. Klymko, E. D. Perfecto, A. G. Merryman, K. A. Kelly, S. Purushothaman, S. J. Koester, R. Wisnieff, and W. Haensch, "A 300-mm wafer-level three-dimensional integration scheme using tungsten through-silicon via and hybrid Cu-adhesive bonding," in *Proc. IEEE Int. Electron Devices Meeting*, San Francisco, CA, USA, Dec. 2008, pp. 1–4, doi: 10.1109/IEDM.2008.4796762.

[37] B. Jiao, J. Qiao, S. Jia, R. Liu, X. Wei, S. Yun, Y. Kong, Y. Ye, X. Du, L. Yu, and B. Cong, "Low stress TSV arrays for high-density interconnection," *Engineering*, vol. 38, pp. 201–208, Jul. 2024, doi: 10.1016/j.eng.2023.11.023.

[38] Y.-C. Chan, N. Basu, T.-W. Chen, Y.-T. Tsai, H.-Y. Lin, S.-C. Chen, M.-H. Lee, and M.-H. Liao, "The analysis of multiwall carbon nanotubes as through silicon via by equivalent circuit model at different operating temperatures in multilayers stacking scheme," *IEEE Trans. Electron Devices*, vol. 70, no. 6, pp. 3360–3364, Jun. 2023, doi: 10.1109/TED.2023.3267762.

[39] G. Luo, Y. Shi, and J. Cong, "An analytical placement framework for 3-D ICs and its extension on thermal awareness," *IEEE Trans. Comput.-Aided Design Integr. Circuits Syst.*, vol. 32, no. 4, pp. 510–523, Apr. 2013, doi: 10.1109/TCAD.2012.2232708.

[40] L. Hou, J. Fu, J. Wang, and N. Gong, "A novel thermal-aware structure of TSV cluster in 3D IC," *Microelectronic Eng.*, vol. 153, pp. 110–116, Mar. 2016, doi: 10.1016/j.mee.2016.03.014.

[41] Y. Zhang, Y. Zhang, and M. S. Bakir, "Thermal design and constraints for heterogeneous integrated chip stacks and isolation technology using air gap and thermal bridge," *IEEE Trans. Compon., Packag., Manuf. Technol.*, vol. 4, no. 12, pp. 1914–1924, Dec. 2014, doi: 10.1109/TCPMT.2014.2364742.

[42] D. H. Kim, K. Athikulwongse, and S. K. Lim, "Study of through-silicon-via impact on the 3-D stacked IC layout," *IEEE Trans. Very Large Scale Integr. (VLSI) Syst.*, vol. 21, no. 5, pp. 862–874, May 2013, doi: 10.1109/TVLSI.2012.2201760.

[43] D. Chaudhuri, D. Nandi Das, H. Rahaman, and T. Ghosh, "Heat mitigation in 3D ICs by improvised TTSV structure," in *Proc. Int. Symp. Devices, Circuits Syst. (ISDCS)*, Howrah, India, Mar. 2020, pp. 1–4, doi: 10.1109/ISDCS49393.2020.9262977.

[44] S. Govind Singh and C. Seng Tan, "Thermal mitigation using thermal through silicon via (TTSV) in 3-D ICs," in *Proc. 4th Int. Microsyst., Packag., Assem. Circuits Technol. Conf.*, Taipei, Taiwan, Oct. 2009, pp. 182–185, doi: 10.1109/IMPACT.2009.5382145.

[45] S. Onkaraiah and C. S. Tan, "Mitigating heat dissipation and thermo-mechanical stress challenges in 3-D IC using thermal through silicon via (TTSV)," in *Proc. 60th Electron. Compon. Technol. Conf. (ECTC)*, Las Vegas, NV, USA, Jun. 2010, pp. 411–416, doi: 10.1109/ECTC.2010.5490939.

[46] S. Hu, Y. Y. G. Hoe, H. Li, D. Zhao, J. Shi, Y. Han, K. H. Teo, Y. Z. Xiong, J. He, X. Zhang, M. Je, and M. Madihian, "A thermal isolation technique using through-silicon vias for three-dimensional ICs," *IEEE Trans. Electron Devices*, vol. 60, no. 3, pp. 1282–1287, Mar. 2013, doi: 10.1109/TED.2013.2243452.

[47] H.-Y. Li, M.-H. Chiang, C.-I. Lee, and W.-J. Yang, "Thermal performance of plate-fin vapor chamber heat sinks," *Int. Commun. Heat Mass Transf.*, vol. 37, no. 7, pp. 731–738, Aug. 2010, doi: 10.1016/j.icheatmasstransfer.2010.05.015.

[48] M. Morega and A. Bejan, "Plate fins with variable thickness and height for air-cooled electronic modules," *Int. J. Heat Mass Transf.*, vol. 37, pp. 433–445, Mar. 1994, doi: 10.1016/0017-9310(94)90043-4.

[49] D.-K. Kim, J. Jung, and S. J. Kim, "Thermal optimization of plate-fin heat sinks with variable fin thickness," *Int. J. Heat Mass Transf.*, vol. 53, nos. 25–26, pp. 5988–5995, Dec. 2010, doi: 10.1016/j.ijheatmasstransfer.2010.07.052.

[50] S. Feng, M. Shi, H. Yan, S. Sun, F. Li, and T. J. Lu, "Natural convection in a cross-fin heat sink," *Appl. Thermal Eng.*, vol. 132, pp. 30–37, Mar. 2018, doi: 10.1016/j.applthermaleng.2017.12.049.

[51] X. Meng, J. Zhu, X. Wei, and Y. Yan, "Natural convection heat transfer of a straight-fin heat sink," *Int. J. Heat Mass Transf.*, vol. 123, pp. 561–568, Aug. 2018, doi: 10.1016/j.ijheatmasstransfer.2018.03.002.

[52] A. R. Sarhan, M. R. Karim, Z. K. Kadhim, and J. Naser, "Experimental investigation on the effect of vertical vibration on thermal performances of rectangular flat plate," *Experim. Thermal Fluid Sci.*, vol. 101, pp. 231–240, Jan. 2019, doi: 10.1016/j.expthermflusci.2018.10.024.

[53] H. E. Ahmed, "Optimization of thermal design of ribbed flat-plate fin heat sink," *Appl. Thermal Eng.*, vol. 102, pp. 1422–1432, Jun. 2016, doi: 10.1016/j.applthermaleng.2016.03.119.

[54] D.-K. Kim, "Thermal optimization of branched-fin heat sinks subject to a parallel flow," *Int. J. Heat Mass Transf.*, vol. 77, pp. 278–287, Oct. 2014, doi: 10.1016/j.ijheatmasstransfer.2014.05.010.

[55] D.-K. Kim, "Thermal optimization of plate-fin heat sinks with fins of variable thickness under natural convection," *Int. J. Heat Mass Transf.*, vol. 55, no. 4, pp. 752–761, Jan. 2012, doi: 10.1016/j.ijheatmasstransfer.2011.10.034.
[56] A. Sakanova and K. J. Tseng, "Comparison of pin-fin and finned shape heat sink for power electronics in future aircraft," *Appl. Thermal Eng.*, vol. 136, pp. 364–374, May 2018, doi: 10.1016/j.applthermaleng.2018.03.020.
[57] J. Hua, G. Li, X. Zhao, and Q. Li, "Experimental study on thermal performance of micro pin fin heat sinks with various shapes," *Heat Mass Transf.*, vol. 53, no. 3, pp. 1093–1104, Mar. 2017, doi: 10.1007/s00231-016-1880-8.
[58] P. Bhandari and Y. K. Prajapati, "Thermal performance of open microchannel heat sink with variable pin fin height," *Int. J. Thermal Sci.*, vol. 159, Jan. 2021, Art. no. 106609, doi: 10.1016/j.ijthermalsci.2020.106609.
[59] R.-T. Huang, W.-J. Sheu, and C.-C. Wang, "Orientation effect on natural convective performance of square pin fin heat sinks," *Int. J. Heat Mass Transf.*, vol. 51, nos. 9–10, pp. 2368–2376, May 2008, doi: 10.1016/j.ijheatmasstransfer.2007.08.014.
[60] W. Al-Sallami, A. Al-Damook, and H. M. Thompson, "A numerical investigation of thermal airflows over strip fin heat sinks," *Int. Commun. Heat Mass Transf.*, vol. 75, pp. 183–191, Jul. 2016, doi: 10.1016/j.icheatmasstransfer.2016.03.014.
[61] A. Al-Damook, N. Kapur, J. L. Summers, and H. M. Thompson, "Computational design and optimisation of pin fin heat sinks with rectangular perforations," *Appl. Thermal Eng.*, vol. 105, pp. 691–703, Jul. 2016, doi: 10.1016/j.applthermaleng.2016.03.070.
[62] M. R. Hajmohammadi, "Optimal design of tree-shaped inverted fins," *Int. J. Heat Mass Transf.*, vol. 116, pp. 1352–1360, Jan. 2018, doi: 10.1016/j.ijheatmasstransfer.2017.09.042.
[63] Y. Zhang, C. R. King, J. Zaveri, Y. J. Kim, V. Sahu, Y. Joshi, and M. S. Bakir, "Coupled electrical and thermal 3D IC centric microfluidic heat sink design and technology," in *Proc. IEEE 61st Electron. Compon. Technol. Conf. (ECTC)*, Lake Buena Vista, FL, USA, May 2011, pp. 2037–2044, doi: 10.1109/ECTC.2011.5898797.
[64] W. M. A. A. Japar, N. A. C. Sidik, R. Saidur, Y. Asako, and S. N. A. Yusof, "A review of passive methods in microchannel heat sink application through advanced geometric structure and nanofluids: Current advancements and challenges," *Nanotechnol. Rev.*, vol. 9, no. 1, pp. 1192–1216, Dec. 2020, doi: 10.1515/ntrev-2020-0094.
[65] H. Tan, L. Wu, M. Wang, Z. Yang, and P. Du, "Heat transfer improvement in microchannel heat sink by topology design and optimization for high heat flux chip cooling," *Int. J. Heat Mass Transf.*, vol. 129, pp. 681–689, Feb. 2019, doi: 10.1016/j.ijheatmasstransfer.2018.09.092.
[66] S. Deldar and M. Khoshvaght-Aliabadi, "Evaluation of water-cooled heat sink with complex designs of groove for application in fusion energy management," *Fusion Eng. Design*, vol. 140, pp. 107–116, Mar. 2019, doi: 10.1016/j.fusengdes.2019.01.149.
[67] L. Chai, L. Wang, and X. Bai, "Thermohydraulic performance of microchannel heat sinks with triangular ribs on sidewalls—Part 1: Local fluid flow and heat transfer characteristics," *Int. J. Heat Mass Transf.*, vol. 127, pp. 1124–1137, Dec. 2018, doi: 10.1016/j.ijheatmasstransfer.2018.08.114.
[68] L. Chai, L. Wang, and X. Bai, "Thermohydraulic performance of microchannel heat sinks with triangular ribs on sidewalls—Part 2: Average fluid flow and heat transfer characteristics," *Int. J. Heat Mass Transf.*, vol. 128, pp. 634–648, Jan. 2019, doi: 10.1016/j.ijheatmasstransfer.2018.09.027.
[69] L. Chai and L. Wang, "Thermal-hydraulic performance of interrupted microchannel heat sinks with different rib geometries in transverse microchambers," *Int. J. Thermal Sci.*, vol. 127, pp. 201–212, May 2018, doi: 10.1016/j.ijthermalsci.2018.01.029.
[70] P.-S. Lee, S. V. Garimella, and D. Liu, "Investigation of heat transfer in rectangular microchannels," *Int. J. Heat Mass Transf.*, vol. 48, no. 9, pp. 1688–1704, Apr. 2005, doi: 10.1016/j.ijheatmasstransfer.2004.11.019.
[71] G. Xia, L. Chai, H. Wang, M. Zhou, and Z. Cui, "Optimum thermal design of microchannel heat sink with triangular reentrant cavities," *Appl. Thermal Eng.*, vol. 31, nos. 6–7, pp. 1208–1219, May 2011, doi: 10.1016/j.applthermaleng.2010.12.022.
[72] W. M. A. A. Japar, N. A. C. Sidik, and S. Mat, "A comprehensive study on heat transfer enhancement in microchannel heat sink with secondary channel," *Int. Commun. Heat Mass Transf.*, vol. 99, pp. 62–81, Dec. 2018, doi: 10.1016/j.icheatmasstransfer.2018.10.005.
[73] I. A. Ghani, N. Kamaruzaman, and N. A. C. Sidik, "Heat transfer augmentation in a microchannel heat sink with sinusoidal cavities and rectangular ribs," *Int. J. Heat Mass Transf.*, vol. 108, pp. 1969–1981, May 2017, doi: 10.1016/j.ijheatmasstransfer.2017.01.046.
[74] Y. F. Li, G. D. Xia, D. D. Ma, Y. T. Jia, and J. Wang, "Characteristics of laminar flow and heat transfer in microchannel heat sink with triangular cavities and rectangular ribs," *Int. J. Heat Mass Transf.*, vol. 98, pp. 17–28, Jul. 2016, doi: 10.1016/j.ijheatmasstransfer.2016.03.022.
[75] E. Bayrak, A. B. Olcay, and M. F. Serincan, "Numerical investigation of the effects of geometric structure of microchannel heat sink on flow characteristics and heat transfer performance," *Int. J. Thermal Sci.*, vol. 135, pp. 589–600, Jan. 2019, doi: 10.1016/j.ijthermalsci.2018.08.030.
[76] W. He, J. Li, and Q. Li, "Optimized design of multilayer embedded micro-fins for enhanced thermal management in three-dimensional stacked chips with heterogeneous heat sources," *Case Stud. Thermal Eng.*, vol. 64, Dec. 2024, Art. no. 105490, doi: 10.1016/j.csite.2024.105490.
[77] S. Kumar and S. Chakrabarti, "A review: Enhancement of heat transfer with nanofluids," *Int. J. Eng. Res.*, vol. 3, no. 4, pp. 549–557, Apr. 2014.
[78] S. P. Jang and S. U. S. Choi, "Cooling performance of a microchannel heat sink with nanofluids," *Appl. Thermal Eng.*, vol. 26, nos. 17–18, pp. 2457–2463, Dec. 2006, doi: 10.1016/j.applthermaleng.2006.02.036.
[79] T.-C. Hung, W.-M. Yan, X.-D. Wang, and C.-Y. Chang, "Heat transfer enhancement in microchannel heat sinks using nanofluids," *Int. J. Heat Mass Transf.*, vol. 55, nos. 9–10, pp. 2559–2570, Apr. 2012, doi: 10.1016/j.ijheatmasstransfer.2012.01.004.
[80] V. Çorumlu, "The effects of input power and ambient temperature on the thermal performance of conical pin fin heat sink in natural convection," *Int. J. Thermal Sci.*, vol. 197, Mar. 2024, Art. no. 108855, doi: 10.1016/j.ijthermalsci.2023.108855.
[81] M. Kopeć and R. Olbrycht, "The influence of air humidity on effectiveness of heat sink work," in *Proc. Int. Conf. Quant. Infr. Thermography*, 2016, pp. 418–423, doi: 10.21611/qirt.2016.061.
[82] S. Singh, A. K. Panigrahi, O. K. Singh, and S. G. Singh, "Analysis of graphene and CNT based finned TTSV and spreaders for thermal management in 3D IC," in *Proc. IEEE Int. 3D Syst. Integr. Conf. (3DIC)*. San Francisco, CA, USA: IEEE, Nov. 2016, pp. 1–4, doi: 10.1109/3DIC.2016.7970000.
[83] A. Barua, M. S. Hossain, K. I. Masood, and S. Subrina, "Thermal management in 3-D integrated circuits with graphene heat spreaders," *Phys. Proc.*, vol. 25, pp. 311–316, Jan. 2012, doi: 10.1016/j.phpro.2012.03.089.
[84] S. K. Vendra and M. Chrzanowska-Jeske, "Thermal management in 3D IC designs for nano-CMOS technologies: Analysis on graphene- vs. graphite-based TIM," in *Proc. IEEE 13th Nanotechnol. Mater. Devices Conf. (NMDC)*, Oct. 2018, pp. 1–4, doi: 10.1109/NMDC.2018.8605929.
[85] T. Brunschwiler, A. Sridhar, C. Lee Ong, and G. Schlottig, "Benchmarking study on the thermal management landscape for three-dimensional integrated circuits: From back-side to volumetric heat removal," *J. Electron. Packag.*, vol. 138, no. 1, Mar. 2016, Art. no. 010911, doi: 10.1115/1.4032492.
[86] H. Oh, Y. Zhang, L. Zheng, G. S. May, and M. S. Bakir, "Fabrication and characterization of electrical interconnects and microfluidic cooling for 3D ICS with silicon interposer," *Heat Transf. Eng.*, vol. 37, no. 11, pp. 903–911, Jul. 2016, doi: 10.1080/01457632.2015.1097753.

FEN GUO received the B.S. degree in microelectronics from Jilin University, in 2015, and the Ph.D. degree in microelectronics and solid state electronics from the University of Chinese Academy of Sciences, in 2021. She is currently an Engineer with Shandong Yunhai Guochuang Cloud Computing Equipment Industry Innovation Company Ltd., Jinan, China. Since 2022, she has been a Postdoctoral Researcher with the Inspur Group. She has a number of quality publications in both national and international conferences and journals. Her research interests include thermal management in 3D IC, advanced packaging, and third generation semiconductor technology.

ZHAO-JUN SUO received the B.S. degree in applied physics from the University of Science and Technology Beijing, Beijing, China, in 2015, and the joint Ph.D. degree in condensed matter physics from the Institute of Semiconductors, Chinese Academy of Sciences, and University of Chinese Academy of Sciences, Beijing, in 2022. She is currently an Engineer with Shandong Yunhai Guochuang Cloud Computing Equipment Industry Innovation Company Ltd., Jinan, China. Her research interests include thermal management in 3D IC, algorithm optimization, and implementation. She focused on semiconductor defect calculation and related methods during her doctoral study.

XIN XI was born in Handan, Hebei, China, in 1987. He received the B.S. degree in material science and technology from Central South University, in 2010, the M.S. degree in material science and technology from Tianjin University, in 2014, and the Ph.D. degree in microelectronics and solid state electronics from Chinese Academy of Science (CAS), in 2020. From 2020 to 2022, he was a Postdoctoral Researcher with Peking University mainly research in condensed matter physics. Since 2022, he has been a Researcher who is engaged in chip design and development with Shandong Yunhai Guochuang Cloud Computing Equipment Industry Innovation Company Ltd. He has published 31 SCI articles in chip design and fabrication. His current research interests include chip design, chip package, and chip fabrication.

YU BI received the B.S. degree in communication engineering from the North University of China, in 2013, and the Ph.D. degree in instrument science and technology, in 2019. She was a Postdoctoral Fellow with Beijing Institute of Technology. Currently, she is a Senior Engineer with Shandong Yunhai Guochuang Cloud Computing Equipment Industry Innovation Company Ltd. Her research interests include chip design, photonic computing chip, and nanophotonic device.

TUO LI received the B.S. degree in computer science and technology from the National University of Defense Technology, in 2008, and the M.S. degree in electrical and electronic engineering from The University of Hong Kong, in 2013. From 2008 to 2011, he was an Engineer with Inspur. Since 2013, he has been a Researcher who is engaged in chip design and development in Inspur. His current research interests include chip design, system architecture and algorithm optimization, and implementation.

CHANGHONG WANG received the B.S. degree in communication engineering and the Ph.D. degree in information and communication engineering from Beijing Institute of Technology, in 2010 and 2020, respectively. Since 2020, he has been an Engineer with Shandong Yunhai Guochuang Cloud Computing Equipment Industry Innovation Company Ltd. His current research interests include hip design, chip synthesis, and system architecture.

KANG SU received the Ph.D. degree in microelectronics and solid state electronics from the University of Chinese Academy of Sciences (UCAS), in 2020. Since 2020, he has been an Engineer with Shandong Yunhai Guochuang Cloud Computing Equipment Industry Innovation Company Ltd. He is currently a Senior Engineer in the field of electronic information. His work focuses on the design of digital integrated circuits, especially the interconnection network on chip and cache coherence protocol.

XIAOFENG ZOU received the B.S. degree in electronic information engineering from Shandong Normal University, in 2011, and the M.S. degree in software engineering from the National University of Defense Technology, in 2014. Since 2014, he has been a Researcher with Inspur. His current research interests include chip design, cache coherence protocol, and computer architecture.

RENGANG LI received the B.S. degree in communication engineering from China University of Petroleum, in 2005, and the M.S. degree in software engineering from the National University of Defense Technology, in 2008. Since 2008, he has been a Researcher with Inspur. He has presided over or participated in six national scientific research projects, applied for 170 patents, authorized 60 Chinese invention patents, authorized nine international invention patents, published 25 articles, and participated in the standard formulation of eight. His current research interests include computer architecture, quantum computing architecture, and chip development. He has won the First Prize of Science and Technology Progress of Shandong Province, the First Prize of Science and Technology Award of China Electronics Society, the Outstanding Award of Science and Technology Progress of China Computer Society, the Excellent Award of China Patent Award, and the Outstanding Young Engineer of Beijing.